DOI: 10.1002/ejic.200600690

Syntheses, Properties and Structures of $[\{(C_5Me_5)_2Nb\}_2NiTe_4]$ and $[(tBuC_5H_4Nb)_2Ni_5Te_7(Ph_2PCH_2PPh_2)_2]$: The Quest for Tetratelluronickelate Clusters

Martin Brandl,[a] Alexander Ebner,[a] Marek M. Kubicki,[b] Yves Mugnier,[b] Joachim Wachter,*[a] Estelle Vigier-Juteau,[b] and Manfred Zabel[a]

Keywords: Niobium / Nickel / Tellurium / Electrochemistry / Density functional calculations

The reaction of $[Ni(COD)_2]$ with $[Cp^*_2NbTe_2H]$ (**1**; Cp^* = η-C_5Me_5) in the presence of $Ph_2PCH_2PPh_2$ (dppm) in boiling toluene gives black-violet $[(Cp^*_2Nb)_2NiTe_4]$ (**3**). If $[Cp'_2NbTe_2H]$ (**2**; Cp′ = $tBuC_5H_4$) is used under similar conditions dark-brown $[(Cp'Nb)_2Ni_5Te_7(dppm)_2]$ (**4**) is formed. The structures of **3** and **4** have been determined crystallographically. Complex **3** contains a severely distorted $NiTe_4$ tetrahedron to which two niobocene groups are coordinated. Density functional analysis of the electronic structure of the $NiTe_4$ building block shows that it is best described as an $[Ni(\eta^2\text{-}Te_2)_2]^{2-}$ fragment. The structure of **4** reveals the presence of two Ni_5 and Te_5 tetragonal pyramids stacked into each other in an opposite way. Six of the Te bridges form two triangular faces, each of which is capped by a Cp′Nb fragment. Additionally, two dppm ligands bridge the long Ni–Ni edges of the Ni_4 bases. Oxidation of **3** with $[(C_5H_5)_2Fe]BPh_4$ gives paramagnetic $[(Cp^*_2Nb)_2NiTe_4]BPh_4$ (**6**), whereas oxidation with $[(C_5H_5)_2Fe]PF_6$ proceeds with fluoride transfer to give $[Cp^*_2NbF_2]PF_6$ (**5**). Electrochemical studies of **3** reveal the existence of the redox couples $[\mathbf{3}]^{2+}/[\mathbf{3}]^{+}/[\mathbf{3}]^{0}/[\mathbf{3}]^{-}/[\mathbf{3}]^{2-}$. Density functional calculations carried out on the different oxidation states of **3** reveal the following main features: the persistent presence of Nb–Ni bonds and the retention of Te–Te bonds in cationic and neutral species and their breaking off in reduced forms. Irrespective of the initial site of electrochemical attack, the Te atoms and Cp rings are principally affected in the final products.

Introduction

The idea of employing tetrachalcogeno metallate anions $[MX_4]^{2-}$ as ligands for the synthesis of heterodimetallic chalcogenido clusters was first elaborated by Müller et al. with M = V, Mo, and W and X = S and Se.[1] Such compounds are of interest as building blocks in extended structures that possess nonlinear optical properties.[2] Little is known about telluro metallates with coordination number four, however.[3] Whereas bis(niobocene)tetrathio and -seleno metallates of formula $[(Cp^*_2Nb)_2MX_4]$ (M = Cr, Mo, Fe, Co; X = S, Se) are easily formed in the reaction between $[Cp^*_2NbE_2H]$ derivatives and the corresponding metal carbonyls,[4,5] $[\{(Cp'_2Nb)_2WTe_4\}W(CO)_4]$ has been synthesised only recently from $W(CO)_6$ and $[Cp'_2NbTe_2H]$ (**2**; Cp′ = $tBuC_5H_4$). This complex contains the hitherto unknown $[WTe_4]^{2-}$ moiety.[6] The versatile abilities of $[Cp^*_2NbTe_2H]$ (**1**) and **2** to serve as tellurium transfer reagents towards transition metal carbonyls has already been reviewed.[7] In this work, we report on the reactions of **1** and **2** with $[Ni(COD)_2]$ in the presence of $Ph_2PCH_2PPh_2$ (dppm). The structures and properties of the mixed early-late transition metal telluride clusters obtained are investigated and the electronic structure of the hitherto elusive $NiTe_4$ structural moiety is investigated in a theoretical study.

Results and Discussion

Syntheses, Properties and Structural Characterisation

Addition of **1** to a yellow solution of $[Ni(COD)_2]$ and half an equivalent of dppm in toluene at room temperature results in an immediate darkening. Attempts to isolate a well-defined product from this solution failed. After refluxing the solution for 18 h black-violet $[(Cp^*_2Nb)_2NiTe_4]$ (**3**) was isolated in 20% yield after chromatographic work-up. The analogous reaction of **2** with $[Ni(COD)_2]$/dppm in boiling toluene gave brown crystals of $[(Cp'Nb)_2Ni_5Te_7(dppm)_2]$ (**4**) after filtration and cooling to –24 °C in a total yield of 11%.

The field desorption (FD) mass spectrum of **3** exhibits the parent ion along with another peak at *m*/*z* 619 (intensity ratio 3:10), which may be attributed to the $[Cp^*_2NbTe_2]$ fragment. The composition of compound **3** is in agreement

[a] Institut für Anorganische Chemie der Universität Regensburg, 93040 Regensburg, Germany
[b] Laboratoire de Synthèse et d'Electrosynthèse Organométalliques, UMR 5188, Université de Bourgogne, 21078 Dijon, France

Supporting information for this article is available on the WWW under http://www.eurjic.org or from the author.

with the elemental analysis. The ^{1}H NMR spectrum of **3** shows a singlet at δ = 1.89 ppm (C_6D_6) for the C_5Me_5 rings. Complex **4** was characterised by means of elemental analysis, FD-MS, and X-ray crystallography. The FD mass spectrum shows the molecular peak of **4** after focussing the scan range at 2380 ± 50 amu. This was necessary to avoid decomposition during routine registration and to increase the sensitivity of the detector (Figure 1). No satisfactory NMR spectra were obtained because of the low solubility of the cluster.

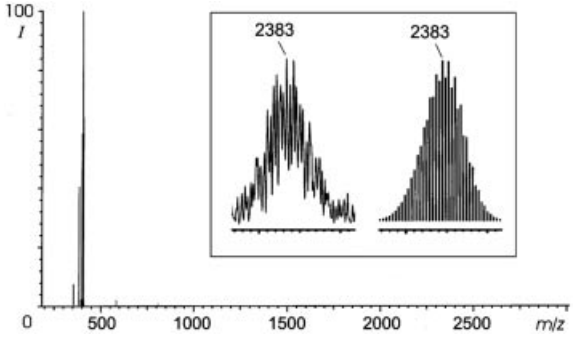

Figure 1. FD mass spectrum of **2** in CH_2Cl_2 (scan range up to 3000 amu). The inset shows the experimental (left) and simulated (right) spectra for a scan range of M ± 50 amu.

Oxidation of **3** with excess $[(C_5H_5)_2Fe]PF_6$ in thf gave yellow $[Cp^*_2NbF_2]PF_6$ (**5**) [Equation (1), path a] according to the FD mass spectrum and elemental analysis. The closely related salt $[(C_5Me_4Et)_2NbF_2]PF_6$ has been prepared previously from $[(C_5Me_4Et)_2NbCl_2]$ by reduction with Na/Hg and subsequent reaction with HPF_6.[8] Similar fluoride-transfer reactions from hexafluorophosphate anion to reactive niobocene derivatives are known.[8,9]

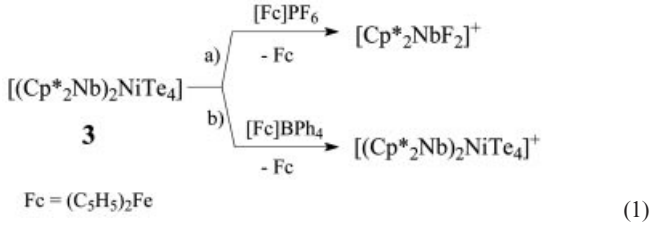

(1)

Reaction of **3** with $[(C_5H_5)_2Fe]BPh_4$, which contains the large and non-coordinating tetraphenylborate anion, was therefore attempted. Black-green $[(Cp^*_2Nb)_2NiTe_4]BPh_4$ (**6**) was formed in 37% yield in thf at room temperature [Equation (1), path b]. The composition was determined by elemental analysis and ESI-MS. The ^{1}H NMR spectrum exhibits a broad singlet at δ = 11.15 ppm, which is in agreement with the expected paramagnetic nature of the new compound. Three multiplets at δ = 7.31, 7.03, and 6.88 ppm may be assigned to the tetraphenylborate anion. Attempts to measure an ESR signal were not successful due to a delocalisation of the unpaired electron over the trimetallic core including the telluride bridges (see below). Unfortunately, single crystals of **6** could not be obtained either.

In another experiment we tried to methylate the Te bridges of **3** with MeI, but $[Cp^*_2NbI_2]$ was obtained as the only product. This means that the lone pairs of the Te bridges are less accessible for methyl electrophilic attack than those in the dinuclear complex $[Cp'_4Nb_2(\mu\text{-}Te)_2]$, which gives $[Cp'_4Nb_2(\mu\text{-}CH_3Te)_2]^{2+}$ upon methylation.[10]

Structure of [Cp$_4$Nb$_2$NiTe$_4$] (3)*

Compound **3** crystallises as monoclinic black rods. Its molecular structure contains a distorted $NiTe_4$ tetrahedron to which two mutually perpendicular niobocene units are coordinated (Figure 2). Thus, complex **3** is one of the extremely rare coordination compounds incorporating an MTe_4 structural unit and is the first tetratelluronickelate derivative. Another example of a tetratelluro metallate complex is $[(Cp'_2Nb)_2WTe_4{\cdot}W(CO)_4]$,[6] in which a central WTe_4 tetrahedron is surrounded by two niobocene fragments. Interestingly, tetrathionickelates like $[Ni(MoS_4)_2]$[11] and $[Ni(WS_4)_2]$[1] prefer a square-planar arrangement of the sulfur ligands around Ni^{2+}.

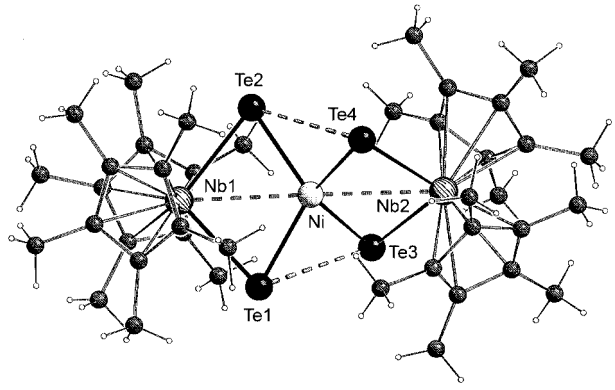

Figure 2. Structure of $[(Cp^*_2Nb)_2NiTe_4]$ (**3**). Selected bond lengths [Å] and angles [°]: Ni–Te 2.470(1)–2.481(1), Nb–Te 2.757(1)–2.766(1), Te1–Te3 3.122(1), Te2–Te4 3.201(1), Ni···Nb1 3.100(4), Ni···Nb2 3.147(4), Te1···Te2 4.212(1), Te3···Te4 4.169(1); Te1–Nb1–Te2 99.2(1), Te1–Ni–Te2 116.4(1), Te1–Ni–Te3 78.2(1), Te2–Ni–Te4 80.5(1), Te1–Ni–Te4 138.2(1), Nb1–Ni–Nb2 178.6(1).

The core of the molecule is characterised by a nearly linear Nb–Ni–Nb arrangement. The Ni–Te distances range from 2.467(1) to 2.481(1) Å and the Nb–Te distances are between 2.757(1) and 2.774(1) Å (see Table S1 in the Supporting Information). The Te–Te distances around Ni merit a more detailed discussion. Taking into account that two $NbTe_2Ni$ rings are linked together by nickel one may distinguish sets of two short and four long Te–Te distances. The latter range between 4.190 and 4.632 Å and are typical of nonbonding intra- and interannular interactions. However, it is striking that the short distances (mean: 3.161 Å) are found between (interannular) Te1 and Te3 and Te2 and Te4 of two different rings.

The geometrical parameters found in both Cp'_2NbTe_2 moieties of **3** differ considerably from those observed in $[Cp'_2Nb(Te_2)H{\cdot}Cr(CO)_5]$.[10] The Te–Nb–Te angle in this compound is contracted to 55.4(1)° and the distance of 2.695(1) Å corresponds well to those reported for side-on terminal η^2-Te_2 ligands in mononuclear complexes for which a Te–Te bond order of between 1 and 2 has been suggested.[12]

The Te–Te distances considered as bonding interactions in a series of complexes comprising the $NiTe_2Ni$ unit vary from 2.802(1) Å in $[\{(triphos)Ni\}_2(\mu\text{-}Te)_2]$[13] to 3.052(5) Å in $[\{(C_5H_iPr_4)Ni\}_2(\mu\text{-}Te)_2]$[14] and even up to 3.28 Å in $[\{CpNi\}_2(\mu_3\text{-}Te)_2\{Ni(PPh_3)Cp\}_2]$.[15] Consequently, the short interannular Te–Te distances observed close to 3.161 Å in the structure of **3** may be considered as long single Te–Te bonds. The question of coupling of two Te atoms coming from two different fragments (interannular) through Ni^{2+} will be discussed in the calculations section below.

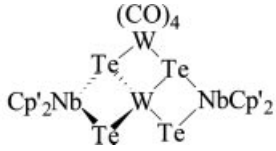

Structure of [(Cp′Nb)$_2$Ni$_5$Te$_7$(dppm)$_2$] (4)

Compound **4** crystallises directly from the filtered reaction mixture as dark prisms. The molecular structure contains a tetragonal pyramid of five nickel atoms at its centre, the basal plane of which is formed by two short (av. 2.637 Å) and two long (av. 3.540 Å) Ni–Ni linkages (Figure 3, Table 1). Six edges of the nickel pyramid are bridged by Te ligands such that they form two triangular faces that serve as tridentate chelate ligands for the coordination of both niobium centres (Figure 4). Another tellurium ligand (Te1) bridges the nickel base in a μ_4-fashion and thus serves as the top of a tetragonal Te_5 pyramid which is inverted with respect to the Ni_5 pyramid. The molecule is completed by two dppm ligands that bridge the long Ni–Ni edges of the rectangular nickel base. The axial phenyl rings of these ligands are arranged in two parallel pairs. The loss of one of the tBuC$_5$H$_4$ ligands from the niobocene unit in this reaction is not new as it has been observed previously during the thermal conversion of $[(Cp'_2NbS_2)_2(\mu\text{-}S_5)]$ into $[Cp'_3Nb_3S_{12}]$.[16]

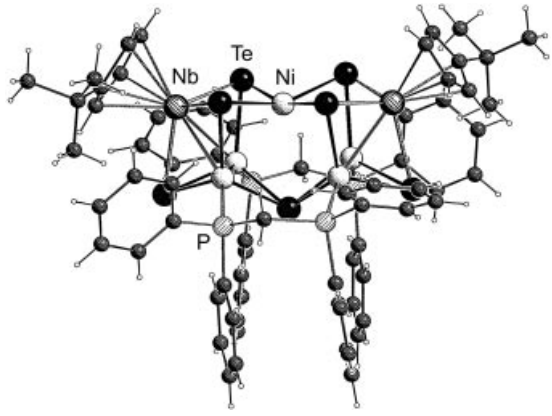

Figure 3. Structure of $[(Cp'Nb)_2Ni_5Te_7(dppm)_2]$ (**4**).

The combination of niobium and nickel atoms together in a polymetallic architecture such as that in **4** is, to the best of our knowledge, unique. The structural motif of the tetragonal d^{10}-metal pyramid is extremely rare; it has been realised previously only in $[Pd_5Se_5(PPh_3)_5]$[17] and $[Ni_5S_4(CH_3CO_2)(PPh_3)_5]^+$.[18]

Table 1. Selected bond lengths [Å] and angles [°] for $[(Cp'Nb)_2Ni_5Te_7{\cdot}2C_7H_8]$ (**4**).

Ni1–Te2	2.563(6)	Ni5–Te1	2.482(5)
Ni1–Te3	2.700(6)	Ni5–Te6	2.551(5)
Ni1–Te5	2.551(6)	Ni5–Te7	2.436(5)
Ni1–Te6	2.634(6)	Ni5–P4	2.252(10)
Ni2–Ni3	2.631(7)	Nb1–Te2	2.640(4)
Ni2–Nb1	2.832(6)	Nb1–Te3	2.686(4)
Ni2–Te2	2.529(5)	Nb1–Te4	2.699(4)
Ni2–Te1	2.549(5)	Nb2–Te5	2.629(4)
Ni2–Te4	2.570(5)	Nb2–Te6	2.722(4)
Ni2–P1	2.120(10)	Nb2–Te7	2.676(5)
Ni3–Nb1	2.793(6)	Ni1–Ni2	2.948(6)
Ni3–Te1	2.457(5)	Ni1–Ni3	3.000(6)
Ni3–Te4	2.469(5)	Ni1–Ni4	2.988(6)
Ni3–Te3	2.527(5)	Ni1–Ni5	2.937(6)
Ni3–P3	2.224(10)	Ni2···Ni4	3.530(6)
Ni4–Ni5	2.644(7)	Ni3···Ni5	3.530(6)
Ni4–Nb2	2.820(5)	Ni1···Te1	3.184
Ni4–Te1	2.559(5)	Te2···Te3	4.019
Ni4–Te5	2.487(5)	Te2···Te5	3.213
Ni4–Te7	2.519(5)	Te3···Te6	3.228
Ni4–P2	2.079(10)	Te5···Te6	4.027
Ni5–Nb2	2.806(6)		
Ni2–Te1–Ni3	63.4(2)	Nb1–Te3–Ni1	76.2(2)
Ni2–Te1–Ni4	87.4(2)	Ni1–Te3–Ni3	70.0(2)
Ni2–Te1–Ni5	121.6(2)	Nb1–Te4–Ni2	65.0(2)
Nb1–Te2–Ni1	79.4(2)	Ni2–Te4–Ni3	62.9(2)
Nb1–Te2–Ni2	66.4(2)	Nb2–Te5–Ni1	78.6(2)
Nb2–Te5–Ni4	66.8(2)	Te2–Ni1–Te5	77.8(2)
Nb2–Te6–Ni1	75.5(2)	Te2–Ni1–Te6	158.1(2)
Nb2–Te6–Ni5	64.2(2)	Te2–Ni2–P1	107.1(3)
Nb2–Te7–Ni4	65.7(2)	Te4–Ni2–P1	113.2(3)
Te2–Nb1–Te3	97.9(2)	Nb1–Ni2–P1	145.1(3)
Te2–Nb1–Te4	108.2(2)	Te3–Ni3–P3	97.8(3)
Ni2–Nb1–Ni3	55.8(2)	P1–C1–P2	126.7(10)
Te2–Ni1–Te3	99.5(2)	P3–C2–P4	110.4(7)

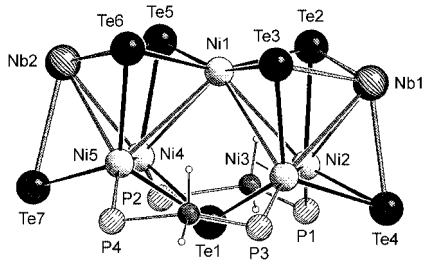

Figure 4. The $Nb_2Ni_5Te_7(P_2CH_2)_2$ core of **4** with labelling scheme.

The cluster core of **4** contains three different ranges of Ni–Ni distances around 2.64 (Ni2–Ni3, Ni4–Ni5), 2.80 (Ni1–Ni2–5), and 3.53 (Ni2–Ni4, Ni3–Ni5) Å. A wide range of Ni–Ni distances (2.49–2.87 Å) of more or less bonding character has been described in the literature, for example in Ni_{10} and Ni_{11} polyhedra.[19] Due to the small covalent radius of nickel (1.15 Å), no bonding interactions are to be expected between Ni2–Ni4 and Ni3–Ni5. On the other hand, the Ni–Nb distances (2.80 Å mean) may be short enough to exhibit a bonding character. Consequently, considering six Ni–Ni and four Ni–Nb metal–metal contacts, each metal centre formally fulfils the 18-electron rule,

although a delocalised bonding situation may be envisaged. Density functional calculations are planned in order to elucidate the electronic structure within the cluster core.

Electrochemical Investigations

The trimetallic sulfido and selenido compounds $[(Cp^*_2Nb)_2MX_4]$ are distinguished by a pronounced redox activity.[4,5] Therefore, and in order to understand the chemical oxidation of **3** by ferricinium salts (see above), we examined the electrochemical behaviour of **3** and **6** in thf solution by rotating disk electrode (RDE) voltammetry, cyclic voltammetry and electrolysis.

The RDE voltammogram of **3** (thf/NBu_4PF_6) exhibits two oxidation waves E′ ($E_{1/2}$ = –0.22 V) and F′ ($E_{1/2}$ = +0.420 V) and three reduction waves A, B, and C (–1.61, –2.12 and –2.25 V, respectively). The heights of waves E′, F′, A and B are nearly equal, whereas wave C is twice as high as B (Figure 5).

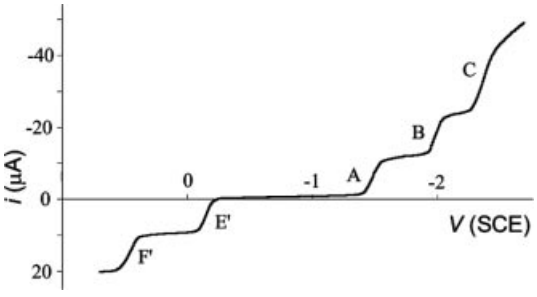

Figure 5. RDE voltammogram of **3** (thf/NBu_4PF_6) at a carbon electrode vs. SCE.

Three reversible systems A/A′, E/E′ and F/F′ are observed at room temperature by cyclic voltammetry (Figure 6). The current ratio $i_{p,a}/i_{p,c}$ for each system is equal to unity (or very close to it) for sweep rates v between 20 and 200 mV s^{-1} and the peak current increases linearly with $v^{1/2}$. The half-wave potential scan rate and the peak shape are characterised by $|E_{p,a} - E_{p,c}| \approx 60$ mV, in agreement with a one-electron transfer controlled by diffusion.[20,21]

Peak B is not reversible at room temperature and an oxidation peak appears at –1.74 V during the anodic scan. At 0 °C a low reversibility (system B/B′) is observed and the intensity of peak B′ increases with the scan rate. These results indicate that the species electrogenerated by one- ($[\mathbf{3}]^+$) or two-electron oxidation ($[\mathbf{3}]^{2+}$) and one-electron reduction ($[\mathbf{3}]^-$) are stable, whereas the product obtained by two-electron reduction ($[\mathbf{3}]^{2-}$) is relatively unstable.

Electrolysis at –1.8 V (plateau of wave A) consumes more than one electron equivalent. After reduction with two electrons the RDE voltammogram of the resulting solution shows the reduction waves A and B and the oxidation waves A′, E′ and F′ (Figure 7, b). After reduction with two and a half electrons wave A decreases and oxidation wave A′ increases (Figure 7, c). It is interesting to note that waves F′, A, A′ and B are nearly as high as the corresponding initial waves, whereas wave E′ is higher. No ESR signal is detected during the electrolysis. The solution shows a slow evolution towards partial regeneration of **3** from $[\mathbf{3}]^-$ upon standing under argon. This means that wave A increases while wave A′ decreases and the height of oxidation wave E′ grows considerably (Figure 7, d). It is still unclear why the formation of $[\mathbf{3}]^-$ consumes more than 1 F. It may well be that this reduction concerns one of the Nb atoms, which means that the anionic charge can be transferred by an intramolecular process to a ligand atom (probably tellurium). Consequently, subsequent oxidation at the potential of wave E′ may give rise to an increase of the height of the concerned oxidation wave.

When oxidative electrolysis is performed at –0.1 V (plateau of wave E′) the current drops to zero after a quantity of electricity of 0.2 F. The RDE voltammogram shows oxidation wave F′ and reduction waves E, A and B (Figure 8). Whereas these waves are in agreement with the formation of the cation $[\mathbf{3}]^+$, two additional reduction waves E_1 and A_1 are observed at –0.86 and –1.86 V, respectively. A similar result has been obtained in CH_2Cl_2/NBu_4PF_6 solution. Under these conditions, 0.2 F was consumed and a 0.2-V shift to more negative potentials is observed for all waves.

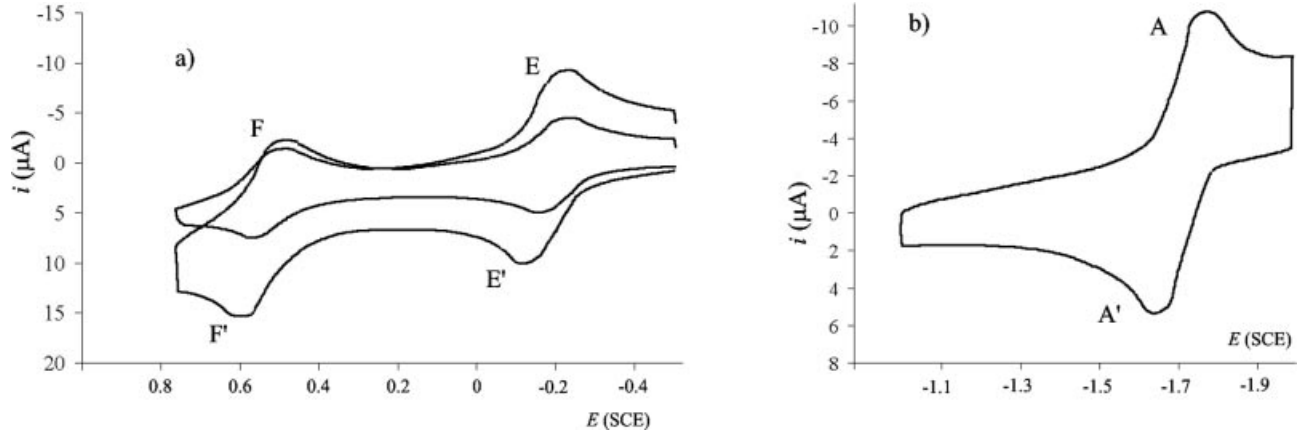

Figure 6. Cyclic voltammogram of **3** (thf/NBu_4PF_6): a) starting potential: –0.5 V; sweep rate: 20 and 100 mV s^{-1}; b) starting potential: –1 V; sweep rate: 50 mV s^{-1}.

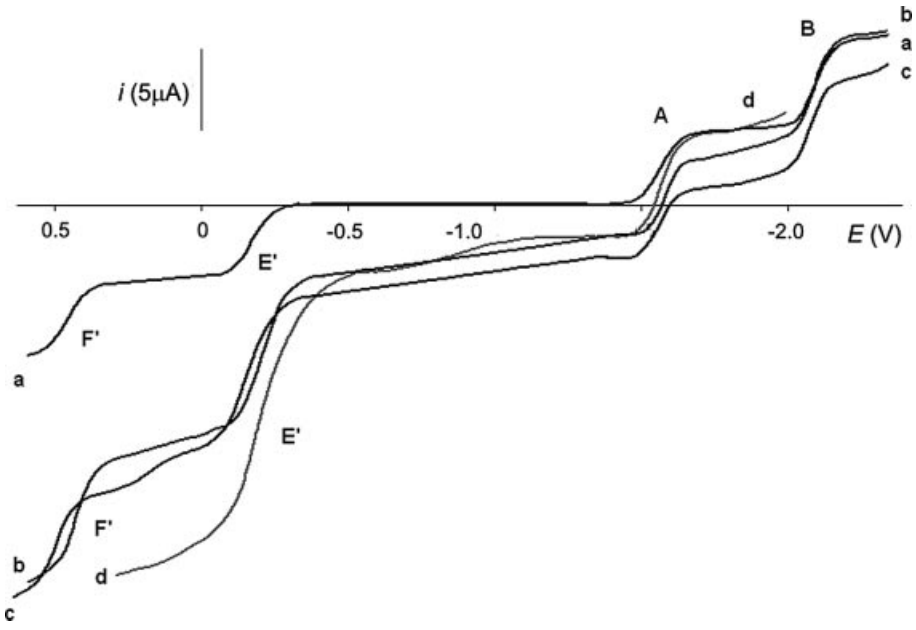

Figure 7. RDE voltammogram of **3** (thf/NBu_4PF_6): a) before electrolysis; b) after two-electron reduction at –1.8 V; c) after consumption of 2.5 F; d) evolution of the reduced solution at room temperature after 1 h.

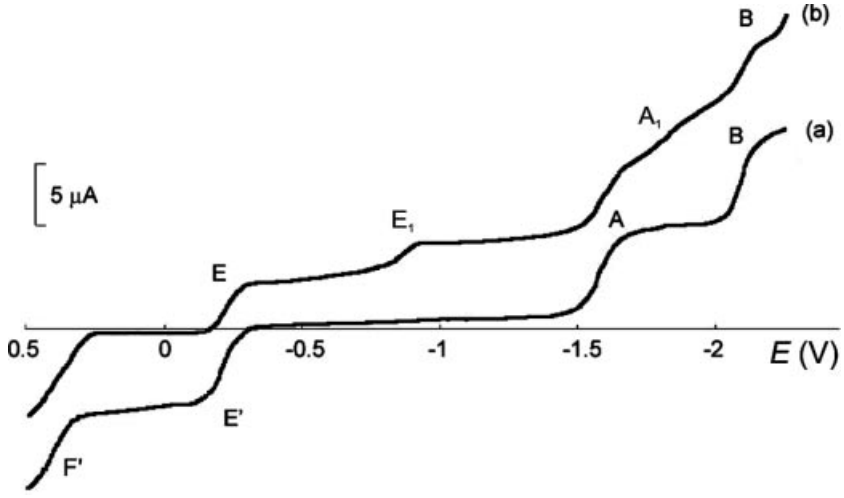

Figure 8. RDE voltammogram of **3** (thf/NBu_4PF_6): a) before electrolysis; b) after oxidation at –0.1 V and consumption of 0.2 F.

It is still unclear why the electrolysis of **3** at –0.1 V consumes 0.2 F instead of the required amount of 1 F for the formation of $[(Cp^*_2Nb)_2NiTe_4]^+$. However, if the oxidation is carried out at +0.35 V (CH_2Cl_2/NBu_4PF_6), 2 F are consumed and the subsequent cyclic voltammograms exhibit two new reversible systems E_1/E_1' and F_1/F_1' at 0.28 and –0.45 V, respectively. These systems may be assigned to the redox couples $[Cp^*_2NbF_2]/[Cp^*_2NbF_2]^+/[Cp^*_2NbF_2]^{2+}$. The first oxidation potential of $[(C_5Me_4Et)_2NbF_2]$ in CH_2Cl_2 has been determined to be $E_{1/2}$ = –0.38 V.[8]

The electrochemical behaviour of $[(Cp^*_2Nb)_2NiTe_4]BPh_4$ (**6**), which contains the cation [**3**]$^+$, was also studied. RDE voltammetry (CH_2Cl_2/NBu_4PF_6) gave the expected oxidation wave F′ at +0.28 V and the reduction wave E at –0.42 V. An additional reduction wave E_1 at –0.86 V is present, as in the case of the electrogenerated cation [**3**]$^+$. The heights of waves F′ and E are nearly equal and are twice as high as wave E_1 (see Figure S1 in the Supporting Information). Two reversible systems F′/F and E/E′ are observed in the cyclic voltammogram.

Density Functional Calculations

The X-ray structure analysis of **3** shows that, contrary to the nearly tetrahedral WTe_4^{2-} bridging fragment in $[\{(Cp'_2Nb)_2WTe_4\}W(CO)_4]$, the $NiTe_4$ moiety is highly distorted with short and long Te–Te distances. It is evident that the nickel atom is unable to reach the formal oxidation state +6 that is plausible for group 6 metals. In order to get an insight into the electronic structure of **3** and of its cationic and anionic species we have carried out DFT calcula-

tions with the Gaussian03 package by using the B3PW91/3-21G (SDD for Nb and Te) functional/basis set couple.[22] The molecular geometries of all systems studied were optimised first and then frequency calculations were performed to confirmation that the optimised geometries correspond well to energy minima. Cp (C_5H_5) replaces Cp* as a ligand in the models.

A preliminary analysis of the electronic properties of $[Cp_2NbTe_2]^-$ and the hypothetical $[NiTe_4]^{2-}$ anionic fragments derived from **3** will be useful for understanding the nature of **3**, and, in particular, why two pairs of Te atoms from two different niobocene ditelluride fragments form Te–Te bonds in the presence of Ni^{2+}.

Formally, complex **3** is built from Ni^{2+} and two chelating $[Cp^*_2NbTe_2]^-$ anions. The electronic structures of bent metallocenes are well known.[23] We should recall, however, the main features of $[Cp_2NbTe_2]^-$ together with the shapes of the frontier molecular orbitals depicted in Figure 9. HOMO–5 to HOMO–3 are responsible for the σ and π Nb–Te bonds based on classical $1a_1$, b_2 and $2a_1$ bent metallocene molecular orbitals,[23] respectively, while HOMO–2 to HOMO are representative of Te lone pairs. Both LUMOs contain a large contribution from Nb atomic orbitals. All depicted orbitals may be involved in Te–Ni and Nb–Ni interactions upon formation of the trimetallic complex **3**. The optimised Nb–Te (2.722 Å), Te–Te (4.193 Å, labelled *intra*annular in **3**) and Te–Nb–Te (101.6°) parameters for $[Cp_2NbTe_2]^-$ are close to the corresponding values found in the crystal structure of **3**.

As shown above, the central $[NiTe_4]^{2-}$ moiety in the structure of **3** is severely distorted. In an attempt to clarify this feature we looked at the behaviour of the hypothetical $[NiTe_4]^{2-}$ anion in planar (D_{4h} and D_{2h}), tetrahedral (T_d) and distorted tetrahedral (D_{2d}) symmetries in the singlet (s) and triplet (tr) spin states. The D_{4h} initial geometry was ruled out because no convergence could be reached upon its optimisation. Remember that the $[NiX_4]^{n-}$ moiety (X = chalcogen) is extremely electron rich and is not known in classical mineral salts. Its stabilisation may occur with electron-withdrawing counterions like selected organometallic buffers. A niobocene seems to be a good candidate, as shown in this paper. Ni^{2+} may exhibit its spin flexibility in distorted polyhedra, which is why both the singlet and triplet states were calculated. The geometry optimisations led to slightly C_{3v} distorted (singlet) and to severely distorted C_1 (triplet) symmetries starting from tetrahedral T_d, and to approximately D_2-symmetric structures starting from D_{2h} and D_{2d} for both the singlet and triplet states. The total energies of the four main species obtained from geometry optimisations increase in the order D_2(tr) (0) < C_1(tr) (0.71) < D_2(s) (1.98) < C_{3v}(s) (2.84 eV). The triplet paramagnetic states are therefore more stable than the diamagnetic singlets. Due to the lack of experimental (e.g. magnetic) data for hypothetical $[NiTe_4]^{2-}$ we did not look at the nature of its singlet and triplet states and can therefore only state that the metal (Ni) must be responsible for them. In fact, in both the singlet and triplet D_2 optimised structures there are two short Te–Te bonding distances [mean: 2.970 (singlet) and 2.987 Å (triplet)] corresponding to the short *inter*annular ones in **3** and two sets of long separations (mean: 4.482/5.138 Å and 5.038/5.137 Å for singlet and triplet, respectively) that correspond to pairs of two long *inter*- and of two *intra*annular Te–Te distances in **3**. Thus, we can conclude that there are two ditelluride (Te_2^{2-}) ligands bound to the Ni^{2+} centre in $[NiTe_4]^{2-}$.

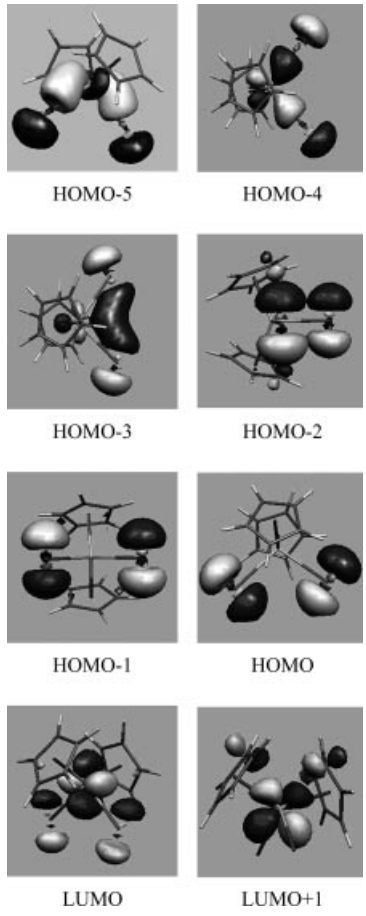

Figure 9. Shapes of significant molecular orbitals of the $[Cp_2NbTe_2]^-$ anion.

Such an intrinsic property of the $[NiTe_4]^{2-}$ anion, which is better described as bis(ditelluro)nickelate $[Ni(Te_2)_2]^{2-}$, in either the singlet or triplet spin state corroborates well the crystal structure of **3**. Selected molecular orbitals of $[Ni(Te_2)_2]^{2-}$ (singlet) are shown in Figure 10. The HOMO–11 and HOMO–3 are the Te–Te bonding orbitals, whereas the HOMO–7 and HOMO–2 may be considered as the non-bonding lone pairs of the Te atoms. Their shapes correspond to the HOMO–2 and HOMO–1 of the $[Cp_2NbTe_2]^-$ anion (Figure 9).

What do we know about the covalency of the Te–Te interaction in pertelluride (Te_2^{2-})? X-ray data suggest a range of 2.67 to 3.05 Å for Te–Te bonds in Te_2^{2-},[12–14,24] and covalent Te–Te bonds in the range of 2.74 to 2.93 Å have been reported from theoretical studies carried out on H_2Te_2 and Me_2Te_2.[25–27] We have calculated (B3WP91/SDD functional/basis set used in this paper) the Te–Te bond lengths for the singlet (2.946 Å) and triplet (3.364 Å) states of free

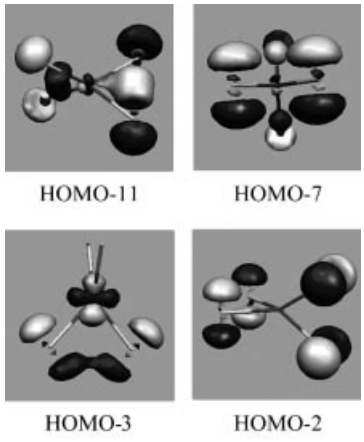

Figure 10. Shapes of selected molecular orbitals of $[Ni(Te_2)_2]^{2-}$.

ditelluride Te_2^{2-}. The triplet state consists of excitation of one electron from a π* antibonding to the high energy σ* orbital of Te_2^{2-}. The calculated Te–Te distance of 2.946 Å in the free diamagnetic molecule increases slightly to 2.970 Å in the diamagnetic complex $[Ni(Te_2)_2]^{2-}$ (vide supra) and up to 3.16 Å in trimetallic **3** (X-ray). In such a trimetallic environment of Te_2^{2-} a lengthening and weakening of the Te–Te bond with retention of its covalent nature is acceptable for **3**. However, one may easily formulate a doubt about its existence at the distances (as long as 3.36 Å) calculated for the triplet state of free Te_2^{2-} and the $[\mathbf{3}]^-$ anion (3.34 Å; vide infra). We checked this last question in the frame of Bader's AIM theory[28] for Te_2^{2-} singlet and triplet states by using a full electron polarised 3-21G* basis set (needed for topological analysis of the wave function) coupled with the B3WP61 functional. The new optimised Te–Te distances are 2.865 (singlet) and 3.400 Å (triplet). Local topological properties such as electron density (ρ, e Å^{-3}), laplacian ($\nabla^2\rho$, e Å^{-5}), density of total energy H (H_a, Å^{-3}) and derived "bond degree" $-H/\rho$ (H_a/e) at bond critical points (BCP) are useful for our purpose. In a simplified approach the covalent interaction needs accumulation of ρ and a negative value of H at the BCP. The $\nabla^2\rho$ may be negative (pure covalent shared–shared interaction) or positive [partially covalent shared–closed interaction; the closed–closed one (H positive) is of a van der Waals or ionic nature]. All considerations of atom–atom interactions need the detection of a BCP. This is the case for both the singlet and triplet states of Te_2^{2-}. The numerical values of ρ, $\nabla^2\rho$, H and $-H/\rho$ at BCPs for the singlet/triplet are 0.37/0.17, –0.02/+0.72, –0.105/–0.012 and 0.28/0.07, respectively. These values also suggest a clearly covalent Te–Te bond in the singlet as some of its covalent nature is retained at a distance as long as 3.4 Å.

The initial geometry obtained from the DFT calculations on $[\mathbf{3}]^0$ is that of the X-ray structure of **3**. The optimisation of $[\mathbf{3}]^{2-}$ leads to one imaginary frequency (excited transition state) and will be only briefly mentioned below. The fact that we were not able to optimise the geometry of the ground state for $[\mathbf{3}]^{2-}$ agrees with the electrochemical evidence for its relative instability. Some metric, charge and energy data for the optimised structures of **3** in different oxidation states are given in Table S2 (see Supporting Information). On comparing the calculated and experimental metric parameters one can clearly see that the $NbTe_2Ni$ rings in $[\mathbf{3}]^0$ are compressed along the Nb–Ni vector by some 0.4 Å and stretched by 0.35 Å along the Te–Te *inter*annular vector with respect to **3** (X-ray). Thus, the direct Nb–Ni bonding interaction is favoured in the isolated molecule over the same molecule packed in the crystal. The shape of the HOMO–4 of **3**, which is clearly an Nb–Ni bonding orbital, is shown in Figure 11. The differences of other heavy atom distances between the calculated $[\mathbf{3}]^0$ and experimental **3** (X-ray) structures are close to 0.05 Å for mean values.

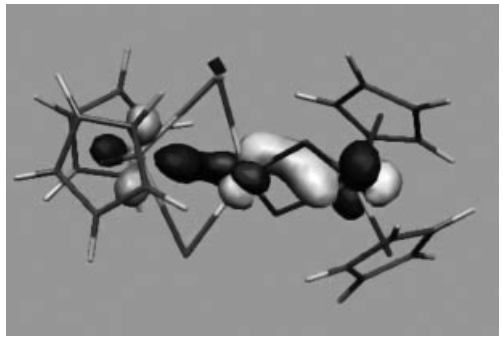

Figure 11. Shape of the HOMO–4 (Nb–Ni–Nb bonding) in the neutral complex **3**.

In the optimised $[\mathbf{3}]^n$ (n = +2, +1, 0, –1) structures the calculated Nb–Ni, Nb–Te, Ni–Te, Te–Te (*intra*) and long Te–Te (*inter*) distances vary in an irregular manner, whereas the short Te–Te (*inter*) (ditelluride Te_2^{2-}) bonds increase regularly on going from $[\mathbf{3}]^{2+}$ to $[\mathbf{3}]^-$. A smooth increase is also observed for cationic and neutral species (mean values of 2.961, 3.040 and 3.105 Å), while a spectacular lengthening of the Te1–Te3 distance up to 3.908 Å is calculated for the anion. Note that the second *inter*annular (Te2–Te4) bond in $[\mathbf{3}]^-$ is also elongated, but "only" to 3.328 Å (Figure 12).

In all $[\mathbf{3}]^n$ species the Nb atoms bear a high positive charge, while the Ni atoms are negatively charged (except in $[\mathbf{3}]^+$). However, the variations of these charges (like those of metric parameters including Nb and Ni) do not correlate with the overall charges. It is, however, worth noting that the sums of metallic charges for all $[\mathbf{3}]^n$ (n = +2, +1, 0, –1) species cover a narrow range of 2.38 ($[\mathbf{3}]^+$) to 2.08 Å ($[\mathbf{3}]^0$). On the other hand, the evolution of Mulliken charges on four Te atoms and four Cp rings follows the overall charges of $[\mathbf{3}]^{2+}$ to $[\mathbf{3}]^-$ species well. This is not surprising for the rings because of their well-known buffer properties. In the case of Te atoms, the observed trend strongly suggests that, whatever the first site of redox processes, the Te atoms are most affected in the final reduced or oxidised structure. Such an overview of the main metric and charge properties of $[\mathbf{3}]^n$ species argues well for the presence of two ditelluride Te_2^{2-} ligands in complexes with n = +2, +1 and 0, where

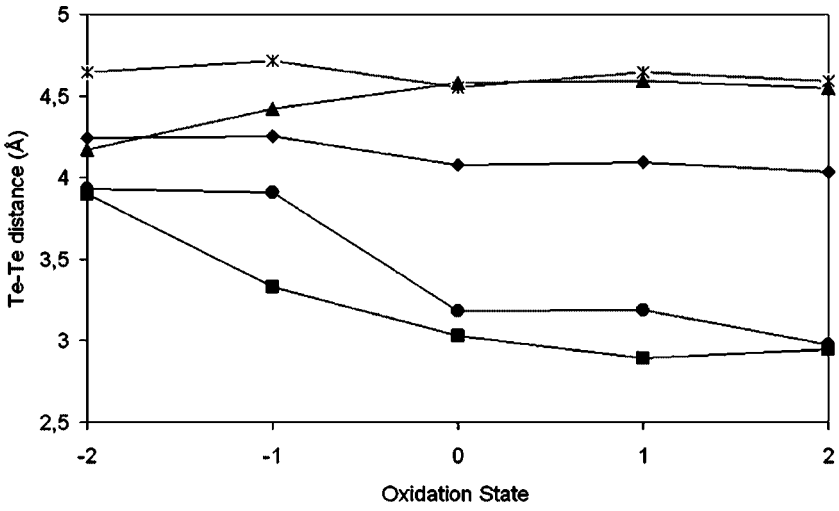

Figure 12. Evolution of the Te–Te distances in differently charged **3**: ■ Te2–Te4 *inter*annular short; ● Te1–Te3 *inter*annular short; ▲ mean of two *inter*annular long (Te1–Te4 and Te2–Te4); ♦ mean of all six Te–Te; × mean of two *intra*annular (Te1–Te2 and Te3–Te4).

the calculated Te–Te distances range between 2.894 and 3.186 Å. The presence of one ditelluride (calculated 3.328 Å) is also expected in the reduced $[\mathbf{3}]^-$ anion from both the tendencies observed in Figure 12 and from the AIM calculations. It is worth noting that the shortest Te–Te distances calculated for the transition state of doubly reduced $[\mathbf{3}]^{2-}$ are 3.896 and 3.929 Å, thus excluding any covalent Te–Te bonding interaction.

Electrochemical studies have revealed the presence of the redox-couples $[\mathbf{3}]^{2+}/[\mathbf{3}]^+$, $[\mathbf{3}]^+/[\mathbf{3}]$ and $[\mathbf{3}]/[\mathbf{3}]^-$ with $E_{1/2}$ potentials of +0.42, –0.22 and –1.61 V, respectively. These values should correlate with the energies (total, HOMO, LUMO) of the implied species. Taking the total energy of neutral $[\mathbf{3}]^0$ as the origin, those of $[\mathbf{3}]^{2+}$, $[\mathbf{3}]^+$ and $[\mathbf{3}]^-$ are equal to +13.979, +4.614 and –1.761 eV, respectively. There is a very good linear correlation between the total energy difference, ΔE_{tot}, values (+9.365, +4.614 and –1.761 eV) and $E_{1/2}$ potentials (linear regression $R^2 = 0.997$) for the three redox systems. On the other hand, the linear correlation does not hold too well for $E_{1/2}$ or the energies of the HOMOs (oxidation, three points, $[\mathbf{3}]^+$, $[\mathbf{3}]^0$, $[\mathbf{3}]^-$, $R^2 = 0.927$) or the LUMOs {reduction, four points, $[\mathbf{3}]^{2+}$, $[\mathbf{3}]^+$, $[\mathbf{3}]^0$ and $[\mathbf{3}]^-$ (with $E_{1/2}$ $[\mathbf{3}]^-/[\mathbf{3}]^{2-} = -2.12$ V), $R^2 = 0.953$}. This may suggest that the one-electron oxidation of $[\mathbf{3}]^0$ does not necessarily operate on its HOMO similar to the one-electron reduction on its LUMO. Other occupied or empty orbitals may contribute to redox processes.

Conclusions

The novel heterometallic telluride clusters $[(Cp^*_2Nb)_2NiTe_4]$ (**3**) and $[(Cp'Nb)_2Ni_5Te_7(dppm)_2]$ (**4**) have been obtained by the reaction of $[Ni(COD)]_2$ with $[Cp^*_2NbTe_2H]$ and $[Cp'_2NbTe_2H]$, respectively. Whereas the presence of the chelating phosphane dppm seems to increase the yields of **3**, it is essential for the formation of cluster **4**. The structure of the latter compound is characterised by two tetragonal Ni_5 and Te_5 pyramids stacked into each other.

Complex **3** is the first example of the trimetallic series $[(Cp^*_2Nb)_2MX_4]$ to contain a formally electron-rich tetratelluronickelate bridge. Contrary to some other experimentally observed tetrahedral MX_4 systems (M = Mo, W; X = S, Se, Te), the DFT calculations provide evidence for the presence of ditelluride ligands as an intrinsic property of the $[NiTe_4]^{2-}$ anion. The calculated Te–Te single bond lengths cover the range from 2.946 to 3.186 Å for $[\mathbf{3}]^{2+}$, $[\mathbf{3}]^+$ and $[\mathbf{3}]^0$, and are as high as 3.328 Å for the $[\mathbf{3}]^-$ anion. It follows from these calculations that the neutral complex **3** does not result from a simple chelation of two $[Cp^*_2NbTe_2]^-$ anions by Ni^{2+}. Instead, its formation is assisted by direct Nb–Ni interactions and bonding Te–Te interactions between both $[Cp^*_2NbTe_2]^-$ anions (*inter*annular bonds). A good linear correlation between the $E_{1/2}$ redox potentials and total energies of different oxidation states of **3** indicates that the electronically delocalised heavy atom core governs these reactions. However, the Te–Te bonding is most affected and thus plays a crucial role in redox processes involving **3**.

Experimental Section

All manipulations were carried out under inert atmosphere using Schlenk line and/or glovebox techniques and dry solvents. Elemental analyses were performed at the Mikroanalytisches Laboratorium, University of Regensburg. IR spectra were obtained with a Mattson Genesis Series FTIR instrument; ESI mass spectra and FD mass spectra were measured with Finnigan TSQ 7000 and MAT 95 instruments, respectively. The ^{1}H- NMR spectra were recorded with a Bruker ARX 250 instrument. $[Cp^*_2NbTe_2H]$ (**1**),[29] $[Cp'_2NbTe_2H]$ (**2**),[10] $[Ni(COD)_2]$[30] and $[(C_5H_5)_2Fe]BPh_4$[31] were prepared as described in the literature. Electrochemical experiments were carried out as described previously.[10]

Synthesis of $[(Cp^*_2Nb)_2NiTe_4]$ (3): $[Ni(COD)_2]$ (110 mg, 0.4 mmol) and dppm (80 mg, 0.2 mmol) were dissolved in toluene (120 mL) and a solution of **1** (250 mg, 0.4 mmol) in 15 mL of toluene, was added. The resulting mixture was stirred for 18 h at 110 °C. After cooling, the solvent was evaporated and the dark residue dissolved

in toluene/pentane (2:1, 15 mL). Chromatography on SiO_2 (column: 15 cm; diameter: 3 cm) gave an orange band containing some **1** upon elution with toluene/pentane (2:1) and then a broad black-violet band containing **3** (100 mg, 20% yield) with toluene. Recrystallisation from toluene/pentane (1:1) gave black crystals. Complex **3**: $C_{40}H_{60}Nb_2NiTe_4{\cdot}C_7H_8$ (1387.98): calcd. C 40.67, H 4.94; found C 40.94, H 4.96. FD-MS (from toluene): *m*/*z* 1296.7 (centre; M^+). ^1H NMR (C_6D_6): δ = 1.89 (s) ppm.

Synthesis of $[(Cp'Nb)_2Ni_5Te_7(dppm)_2]$ (4): A solution of **2** (160 mg, 0.27 mmol) in toluene (20 mL) was added to a yellow solution of $[Ni(COD)_2]$ (150 mg, 0.55 mmol) and dppm (104 mg, 0.27 mmol) in toluene (100 mL). The dark mixture was stirred for 18 h at 110 °C. After cooling, the solution was concentrated to 20 mL and filtered through a frit charged with dry kieselguhr. Then filtrate was then layered carefully with pentane (20 mL). Crystallisation at –20 °C gave several crops of black crystals with a total yield of 11%. Complex **4**: $C_{68}H_{70}Nb_2Ni_5P_4Te_7{\cdot}2C_7H_8$ (2567.94): calcd. C 38.35, H 3.38; found C 37.54, H 3.34. FD-MS (from CH_2Cl_2): *m*/*z* 2383.4 (centre; M^+).

Reaction of 3 with $[Cp_2Fe]PF_6$: A solution of **3** (200 mg, 0.15 mmol) in thf (20 mL) was mixed with a suspension of $[(C_5H_5)_2Fe]PF_6$ (100 mg, 0.30 mmol) in 15 mL of thf. After stirring for 2 h at room temperature a black precipitate separated from the yellow solution. After evaporation of the solvent the residue was suspended in toluene, transferred to a frit charged with Celite® and washed several times with toluene. Dissolving the residue in thf and evaporation of the solvent gave 40 mg (24%) of yellow $[Cp^*_2NbF_2]PF_6$ (**5**). The product is identical with a sample prepared from $[Cp^*_2NbCl_2]$ by reduction with Na/Hg and subsequent reaction with HPF_6.[8] Complex **5**: $C_{20}H_{30}F_8NbP$ (546.32): calcd. C 43.97, H 5.53; found C 43.83, H 5.43. FD-MS (from CH_2Cl_2): *m*/*z* 401.3 $[Cp^*_2NbF_2]^+$. ^1H NMR (CD_2Cl_2): δ = 2.13 (s) ppm.

Synthesis of $[(Cp^*_2Nb)_2NiTe_4]BPh_4$ (6): Complex **3** (250 mg, 0.24 mmol) was dissolved in thf (50 mL) and then added to a suspension of $[(C_5H_5)_2Fe]BPh_4$ (250 mg, 0.49 mmol) in 40 mL of thf. During the reaction the colour changed from black-violet to black-green. After stirring for 4 h at room temperature the solvent was removed. The residue was then washed with toluene (20 mL) to remove $[(C_5H_5)_2Fe]$ (50 mg, 0.27 mmol). The black residue was suspended in thf, filtered and the solvents evaporated to dryness to give 120 mg (37%) of **6**. Repeated recrystallisation from thf gave only microcrystalline material. Complex **6**: $C_{64}H_{80}BNb_2NiTe_4$ (1615.06): calcd. C 47.60, H 5.00; found C 47.31, H 4.84. ESI-MS (from CH_2Cl_2): Positive ion ESI: *m*/*z* 1295.7 $[\mathbf{6}]^+$; negative ion ESI: *m*/*z* 319.0 $[BPh_4]^-$. ^1H NMR (CD_2Cl_2): δ = 11.15 (br. s, 60 H, C_5Me_5), 7.31 (m, 8 H, C_6H_5), 7.03 (m, 8 H, C_6H_5), 6.88 (m, 4 H, C_6H_5) ppm.

Crystal Structure Determination

Complex 3: Black rods were grown from a toluene solution at –24 °C. Data were collected at 173 K on a STOE imaging plate diffraction system (IPDS) using Mo-K_α radiation (λ = 0.71073 Å). Crystallographic details are listed in Table 2. The structure was solved by direct methods and refined by full-matrix least-squares (SHELXL-97) with all reflections. All non-hydrogen atoms were refined with anisotropic displacement parameters. The H atoms were calculated geometrically and a riding model was used during the refinement process.

Complex 4: Crystal data were collected at 123 K on a STOE IPDS instrument using Mo-K_α radiation (λ = 0.71073 Å). Crystallographic details are listed in Table 2. The space group determination following systematic extinction rules for the reflections together with the orthorhombic lattice constants led to space group *Pccn* (no. 56). First attempts to solve the structure by direct methods (SIR-97) immediately showed all heavy atoms. Searching for the carbon atoms by difference Fourier synthesis (SHELX-97) revealed that the chosen symmetry was too high. Inspection of the systematic absence violations of the reflections showed that all violations concern *h*0*l* reflections. Therefore, all following calculations were carried out in the acentric space group $Pc2_1n$, the unconventional setting of $Pna2_1$ (no. 33). In this space group there was no problem to locate all atoms by difference Fourier synthesis. Due to the high degree of pseudo-centrosymmetry and the fact that the crystal was an inversion twin with a ratio of 44:56, the correlation factors between a great number of atomic parameters made several constraints during the refinement calculations necessary. All carbon rings were fitted by the suitable AFIX instruction to a regular hexagon or pentagon, respectively. In particular, the C–C distances of one *tert*-butyl group had to be fixed. Despite including a damping factor during the least-squares refinements, all carbon atoms had to be refined with isotropic displacement factors. In addition, the solvent molecules showed severe positional disorder and could only be refined as a cloud of electron density. The shape of that cloud and the found electron numbers suggested that the solvent molecules are toluene. Despite these difficulties a reliable structure determination was obtained but with slightly increased estimated standard deviations for the interatomic distances.

Table 2. Crystal data for compounds **3** and **4**.

	$[\mathbf{3}]{\cdot}C_7H_8$	$[\mathbf{4}]{\cdot}2C_7H_8$
Formula	$C_{40}H_{60}Nb_2NiTe_4{\cdot}C_7H_8$	$C_{68}H_{70}Nb_2Ni_5P_4Te_7{\cdot}2C_7H_8$
M_w	1387.9	2568.0
Crystal system	monoclinic	orthorhombic
Crystal size [mm]	0.30 × 0.13 × 0.12	0.24 × 0.12 × 0.08
Space group	$P2_1/c$	$Pc2_1n$
a [Å]	9.888(1)	16.156(2)
b [Å]	15.070(1)	21.695(2)
c [Å]	32.416(2)	23.568(2)
β [°]	97.54(1)	
V [Å^3]	4788.4(4)	8260.6(2)
Z	4	2
$\rho_{calcd.}$ [g cm^{-3}]	1.925	2.065
λ Mo-K_α [mm^{-1}]	0.71073	0.71073
T [K]	173	123
Θ range	2.54–25.92	2.34–25.87
Reflections collected	43147	83476
Unique reflections	8839 [*R*(int) = 0.023]	15897 [*R*(int) = 0.100]
Observed reflections [$I > 2\sigma(I)$]	7469	6321
Parameters refined	487	416
Absorption correction	numerical	analytical
Transmission	0.649/0.588	0.613/0.445
Max./min. residual density [e Å^{-3}]	1.006/–0.624	1.548/–0.854
*R*1	0.026	0.053
*wR*2	0.067	0.110

CCDC-610345 (for **3**) and -610346 (for **4**) contain the supplementary crystallographic data for this paper. These data can be obtained free of charge from The Cambridge Crystallographic Data Centre via www.ccdc.cam.ac.uk/data_request/cif.

Supporting Information (see also the footnote on the first page of this article): Selected bond lengths, angles, interatomic distances and energies for redox species for **3**; RDE voltammogram of **6** on carbon electrode.

Acknowledgments

We gratefully acknowledge continuous support over many years from Prof. Dr. H. Brunner and we are grateful to Dr. H. Cattey for her technical assistance. Parts of this work were supported by the Deutsche Forschungsgemeinschaft, the Deutscher Akademischer Auslandsdienst and the Ministère des Affaires Etrangères (program PROCOPE).

[1] A. Müller, E. Diemann, R. Jostes, H. Bögge, *Angew. Chem. Int. Ed. Engl.* **1981**, *20*, 934–955.
[2] a) Q.-F. Zhang, M.-T. Bao, M.-C. Hong, R. Cao, Y.-L. Song, X.-Q. Xin, *J. Chem. Soc., Dalton Trans.* **2000**, 605; b) Q.-F. Zhang, W.-H. Leung, X.-Q. Xin, H.-K. Fun, *Inorg. Chem.* **2000**, *39*, 417 and references cited therein; c) X. Chen, K. Wu, J. G. Snijders, C. Lin, *Inorg. Chem.* **2003**, *42*, 532–540.
[3] a) M. A. Ansari, J. C. Bollinger, J. A. Ibers, *J. Am. Chem. Soc.* **1993**, *115*, 3838–3839; b) M. A. Ansari, J. M. McConnachie, J. A. Ibers, *Acc. Chem. Res.* **1993**, *26*, 574–578.
[4] H. Brunner, M. M. Kubicki, G. Gehart, E. Lehrl, D. Lucas, W. Meier, Y. Mugnier, B. Nuber, B. Stubenhofer, J. Wachter, *J. Organomet. Chem.* **1996**, *510*, 291–295.
[5] O. Blacque, H. Brunner, M. M. Kubicki, D. Lucas, W. Meier, Y. Mugnier, B. Nuber, B. Stubenhofer, J. Wachter, *J. Organomet. Chem.* **1998**, *564*, 71–79.
[6] H. Brunner, J. Wachter, R. Wanninger, M. Zabel, *Eur. J. Inorg. Chem.* **2001**, 1151–1154.
[7] J. Wachter, *Eur. J. Inorg. Chem.* **2004**, 1367–1378.
[8] H. Brunner, G. Gehart, W. Meier, J. Wachter, A. Riedel, S. Elkrami, Y. Mugnier, B. Nuber, *Organometallics* **1994**, *13*, 134–140.
[9] H. Brunner, J.-C. Leblanc, D. Lucas, W. Meier, C. Moise, Y. Mugnier, B. Nuber, S. Rigny, A. Sadorge, J. Wachter, *J. Organomet. Chem.* **1998**, *566*, 203–210.
[10] H. Brunner, H. Cattey, D. Evrard, M. M. Kubicki, Y. Mugnier, E. Vigier, J. Wachter, R. Wanninger, M. Zabel, *Eur. J. Inorg. Chem.* **2002**, 1315–1325.
[11] I. Søtofte, *Acta Chem. Scand.* **1976**, *A30*, 157.
[12] a) V. J. Murphy, D. Rabinovich, S. Halkyard, G. Parkin, *J. Chem. Soc., Chem. Commun.* **1995**, 1099 and references cited therein; b) J. M. Fischer, W. E. Piers, L. R. MacGillivray, M. J. Zaworotko, *Inorg. Chem.* **1995**, *34*, 2499–2500.
[13] M. DiVaira, M. Peruzzini, P. Stoppioni, *J. Chem. Soc., Chem. Commun.* **1986**, 374.
[14] H. Sitzmann, D. Saurenz, G. Wolmershäuser, A. Klein, R. Boese, *Organometallics* **2001**, *20*, 700–705.
[15] D. Fenske, A. Hollnagel, K. Merzweiler, *Angew. Chem. Int. Ed. Engl.* **1988**, *27*, 965–966.
[16] H. Brunner, W. Meier, J. Wachter, B. Nuber, M. L. Ziegler, *J. Organomet. Chem.* **1990**, *381*, C7–C12.
[17] D. Fenske, H. Fleischer, H. Krautscheid, J. Magull, C. Oliver, S. Weisgerber, *Z. Naturforsch., Teil B* **1991**, *46*, 1384–1394.
[18] F. Cecconi, C. A. Ghilardi, S. Midollini, A. Orlandini, A. Vacca, *Inorg. Chem. Commun.* **2000**, *3*, 276–280.
[19] a) D. F. Rieck, J. A. Gavney Jr, R. L. Norman, R. K. Hayashi, L. F. Dahl, *J. Am. Chem. Soc.* **1992**, *114*, 10369–10379; b) D. F. Rieck, R. A. Montag, T. S. McKechnie, L. F. Dahl, *J. Chem. Soc., Chem. Commun.* **1986**, 1330–1331; c) P. D. Mlynek, L. F. Dahl, *Organometallics* **1997**, *16*, 1655–1667; d) A. Ceriotti, F. Demartin, B. T. Heaton, P. Ingallina, G. Longoni, M. Manassero, M. Marchionna, N. Masciocchi, *J. Chem. Soc., Chem. Commun.* **1989**, 786–787; e) A. J. Kahaian, J. B. Thoden, L. F. Dahl, *J. Chem. Soc., Chem. Commun.* **1992**, 353–355; f) V. G. Albano, F. Demartin, M. C. Iapalucci, G. Longoni, M. Monari, P. Zanello, *J. Chem. Soc., Dalton Trans.* **1992**, 497–502; g) J. P. Zebrowski, R. K. Hayashi, L. F. Dahl, *J. Am. Chem. Soc.* **1993**, *115*, 1142–1144; h) V. G. Albano, F. Demartin, C. Femoni, M. C. Iapalucci, G. Longoni, M. Monari, P. Zanello, *J. Organomet. Chem.* **2000**, *593–594*, 325–334.
[20] R. W. Murray, C. N. Reitley, *Electroanalytical Principles*, Interscience, New York, **1963**.
[21] R. S. Nicholson, *Anal. Chem.* **1965**, *37*, 1351–1355.
[22] *Gaussian 03, Revision B.05*, M. J. Frisch, G. W. Trucks, H. B. Schlegel, G. E. Scuseria, M. A. Robb, J. R. Cheeseman, J. A. Montgomery Jr, T. Vreven, K. N. Kudin, J. C. Burant, J. M. Millam, S. S. Iyengar, J. Tomasi, V. Barone, B. Mennucci, M. Cossi, G. Scalmani, N. Rega, G. A. Petersson, H. Nakatsuji, M. Hada, M. Ehara, K. Toyota, R. Fukuda, J. Hasegawa, M. Ishida, T. Nakajima, Y. Honda, O. Kitao, H. Nakai, M. Klene, X. Li, J. E. Knox, H. P. Hratchian, J. B. Cross, C. Adamo, J. Jaramillo, R. Gomperts, R. E. Stratmann, O. Yazyev, A. J. Austin, R. Cammi, C. Pomelli, J. W. Ochterski, P. Y. Ayala, K. Morokuma, G. A. Voth, P. Salvador, J. J. Dannenberg, V. G. Zakrzewski, S. Dapprich, A. D. Daniels, M. C. Strain, O. Farkas, D. K. Malick, A. D. Rabuck, K. Raghavachari, J. B. Foresman, J. V. Ortiz, Q. Cui, A. G. Baboul, S. Clifford, J. Cioslowski, B. B. Stefanov, G. Liu, A. Liashenko, P. Piskorz, I. Komaromi, R. L. Martin, D. J. Fox, T. Keith, M. A. Al-Laham, C. Y. Peng, A. Nanayakkara, M. Challacombe, P. M. W. Gill, B. Johnson, W. Chen, M. W. Wong, C. Gonzalez, and J. A. Pople, Gaussian, Inc., Pittsburgh PA, **2003**.
[23] J. W. Lauher, R. Hoffmann, *J. Am. Chem. Soc.* **1976**, *98*, 1729.
[24] P. Böttcher, J. Getzschmann, R. Keller, *Z. Allg. Anorg. Chem.* **1993**, *619*, 476–488.
[25] J. J. BelBruno, *Heteroat. Chem.* **1997**, *8*, 199–202.
[26] R. Berger, C. Van Wüllen, *J. Chem. Phys.* **2005**, *122*, 134316.
[27] J. M. Gonzales, D. G. Musaev, K. Morokuma, *Organometallics* **2005**, *24*, 4908–4914.
[28] R. F. W. Bader, *Atoms in Molecules: A Quantum Theory*, Clarendon Press, Oxford, U.K., **1990**.
[29] O. Blacque, H. Brunner, M. M. Kubicki, B. Nuber, B. Stubenhofer, J. Wachter, B. Wrackmeyer, *Angew. Chem. Int. Ed. Engl.* **1997**, *36*, 351–353.
[30] D. J. Krysan, P. B. Mackenzie, *J. Org. Chem.* **1990**, *55*, 4229–4230.
[31] T. Birchall, I. Drummond, *Inorg. Chem.* **1971**, *10*, 399–401.

Received: July 13, 2006
Published Online: January 16, 2007

